^{12}CO J=2–1 and ^{12}CO J=3–2 observations toward the high-mass protostellar candidate IRAS 20188+3928

Jin-Long Xu and Jun-Jie Wang

National Astronomical Observatories, Chinese Academy of Sciences, Beijing 100012, China; *xujl@bao.ac.cn*
NAOC-TU Joint Center for Astrophysics, Lhasa 850000, China

Abstract We have carried out observations of ^{12}CO J=2–1 and ^{12}CO J=3–2 toward the high-mass protostellar candidate IRAS 20188+3928. Compared with previous observations, the ^{12}CO J=2–1 and ^{12}CO J=3–2 lines both have asymmetric profiles with an absorption dip. The velocity of the absorption dip is $\sim$ 1.0 km s^{-1}. The spectral shape may be caused by rotation. The velocity-integrated intensity map and position-velocity diagram of the ^{12}CO J=2–1 line present an obvious bipolar component, further verifying that this region has an outflow motion. This region is also associated with an HII region, an IRAS source, and an H$_2$O maser. The H$_2$O maser has the velocity of 1.1 km s^{-1}. Compared with the components of the outflow, we find that the H$_2$O maser is not associated with the outflow. Using the large velocity gradient model, we concluded that possible averaged gas densities of the blueshifted lobe and redshifted lobe are 1.0×10^5 cm^{-3} and 2.0×10^4 cm^{-3}, while kinetic temperatures are 26.9 K and 52.9 K, respectively. Additionally, the outflow has a higher integrated intensity ratio ($I_{\text{CO}\,J=3-2}/I_{\text{CO}\,J=2-1}$).

Key words: ISM: individual (IRAS 20188+3928) — ISM: kinematics and dynamics — ISM: molecules — stars: formation

1 INTRODUCTION

IRAS 20188+3928 is a high-mass protostellar candidate (Zhang et al. 2005), located in the region of Cygnus at the position (l, b) = (77.46°, 1.76°) (Little et al. 1988). Estimations for the distance to this source vary from 0.31 to 4 kpc (Little et al. 1988; Palla et al. 1991; Molinari et al. 1996), hence, the luminosity is highly uncertain. A bipolar molecular outflow was discovered in HCO$^+$ J=2–1 and ^{13}CO J=1–0 emission lines in the IRAS 20188+3928 region (Little et al. 1988). They suggested that the outflowing gas has a dense and clumpy nature in the direction from north to southwest, and IRAS 20188+3928 is not obviously associated with a well known stellar cluster or an HII region. Zhang et al. (2005) observed the bipolar outflow in ^{12}CO J=2–1 centered on the IRAS source, roughly in the north-south direction, but their observation did not fully cover the emission from the bipolar outflow. In addition, Varricatt et al. (2010) not only detected the bipolar outflow in the H$_2$ line, but also an additional outflow in the region. Because the outflows in this region are complicated, further observations are needed toward the IRAS 20188+3928 region.

Additionally, IRAS 20188+3928 is associated with a compact molecular cloud (Anglada et al. 1997). An H_2O maser emission was detected by several other investigators (Palla et al. 1991; Brand et al. 1994; Jenness et al. 1995). Several observers detected NH_3 emission (Molinari et al. 1996; Anglada et al. 1997; Jijina et al. 1999), implying that the IRAS source is deeply embedded in the high density gas, which may be the driving source of the bipolar outflow. Jenness et al. (1995) imaged two sources at 450 and 800 μm, agreeing with the position of two 6-cm radio emission sources detected by Molinari et al. (1998), with the brighter and the fainter ones being located northwest of the IRAS position by $4.2''$ and $28.4''$, respectively. Near-infrared polarimetry revealed an illuminating source, about $6''$ north of the IRAS source (Yao et al. 2000). This illuminating source is better centered on the CO outflow than the IRAS source. Accordingly, near-IR images show a cluster of deeply embedded objects towards the center of the IRAS 20188+3928 region, very close to the position of IRAS 20188+3928. The agreement of these positions indicates that the outflow source is located in the cluster (Varricatt et al. 2010). Hence, although there are multiple young stellar objects in the region, the driving source of the bipolar outflow has not been well identified.

In this paper, we have carried out the ^{12}CO J=2–1 and ^{12}CO J=3–2 observations towards the high-mass protostellar candidate IRAS 20188+3928. For the first time, the observations cover the whole area of IRAS 20188+3928 in these frequencies. Clearly north to southwest outflow and possible rotation may be associated with IRAS 20188+3928.

2 OBSERVATIONS

The mapping observations of IRAS 20188+3928 were performed in ^{12}CO J=2–1 and ^{12}CO J=3–2 lines using the KOSMA 3 m telescope at Gornergrat, Switzerland, in November 2009. The half–power beam widths of the telescope at the observing frequencies of 230.538 GHz and 345.789 GHz were $130''$ and $80''$, respectively. The pointing and tracking accuracy was better than $20''$. The medium and variable resolution acousto optical spectrometers had 1501 and 1601 channels, with total bandwidths of 248 MHz and 544 MHz. The channel widths of 165 and 340 kHz corresponded to velocity resolutions of 0.21 and 0.29 km s^{-1}, respectively. The beam efficiency B_{eff} was 0.68 at 230 GHz and 0.72 at 345 GHz. The forward efficiency F_{eff} was 0.93 for all frequencies. Mapping observations were centered at RA (J2000)=$20^h20^m39.30^s$, Dec (J2000)=$39°37'51.90''$ using the on-the-fly mode, and the total mapping area was $11' \times 11'$ with a $1' \times 1'$ grid. The correction for the line intensities to the main beam temperature scale was made using the formula $T_{mb} = (F_{eff}/B_{eff} \times T_A^*)$. The data were reduced using the GILDAS/CLAS [1] package.

The 1.4 GHz radio continuum emission data were obtained from the NRAO VLA Sky Survey (NVSS; Condon et al. 1998).

3 RESULTS AND DISCUSSION

3.1 CO Molecular Spectra

Figure 1 shows the spectra of ^{12}CO J=2–1, ^{12}CO J=3–2, and ^{13}CO J=1–0 at the position of IRAS 20188+3928. The ^{13}CO J=1–0 data are obtained from the Purple Mountain Observatory archive [2]. Each spectrum displays broad line wings. ^{12}CO J=2–1 and ^{12}CO J=3–2 lines present asymmetric profiles with double peaks, while the ^{13}CO J=1–0 line shows a single peak profile. Wu et al. (2010) only detected one compact core from the IRAS 20188+3928 region in the HCN J=1–0 and CS J=2–1 lines, suggesting that there is one velocity component. The profiles of ^{12}CO J=2–1 and ^{12}CO J=3–2 with double peaks may be an indication of absorption. The velocity of an absorption dip is ~ 1.0 km s^{-1}. Rotation could be responsible for the spectral shape (Wu et al. 2005). With
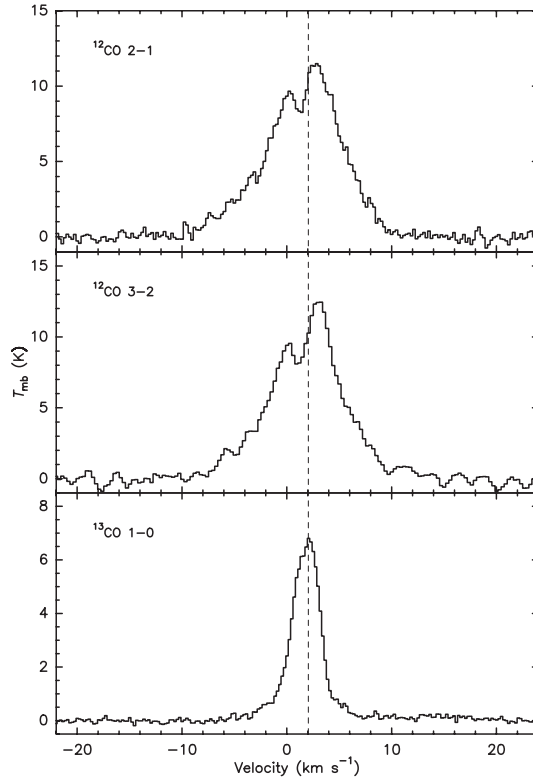
---

[1] *http://www.iram.fr/IRAMFR/GILDAS/*

[2] *http://www.radioast.csdb.cn*

Fig. 1 Spectral profiles observed at the central position of IRAS 20188+3928 in the optically thick ^{12}CO J=2–1 and ^{12}CO J=3–2 lines, and the optically thin ^{13}CO J=1–0 line. The dashed line in the spectra marks the cloud's systemic velocity.

the single-dish data currently available, we did not find any kinematic evidence of rotation. The ^{13}CO J=1–0 line is optically thin, which can be used to determine the systemic velocity. A systemic velocity of ~ 2.0 km s^{-1} is obtained from this line. According to the Galactic rotation model of Fich et al. (1989) together with $R_\odot$ = 8.5 kpc and $V_\odot$ = 220 km s^{-1}, where $V_\odot$ is the circular rotation speed of the Galaxy, we obtain a kinematic distance of 0.32 kpc to IRAS 20188+3928, which is used to calculate the physical parameters in this paper. The full widths (FWs) of the ^{12}CO J=2–1 and ^{12}CO J=3–2 lines are both about 20 km s^{-1} from −10 km s^{-1} to 10 km s^{-1}. The large FWs appear to be a strong indication of outflow motion.

3.2 The Bipolar Outflow

3.2.1 The outflow morphology

To determine the velocity components and morphology of the outflow, we made a position-velocity (PV) diagram with a cut along the north-south direction as shown in Figure 2. The PV diagram in Figure 2 clearly shows bipolar components, but we cannot see the emission from the core of IRAS 20188+3928, indicating that the direction above the cut represents that of the bipolar components. The blueshifted and redshifted components have obvious velocity gradients from −7.6 to −0.6 km s^{-1} and 3.2 to 9.0 km s^{-1}, respectively. The distributions of redshifted and blueshifted
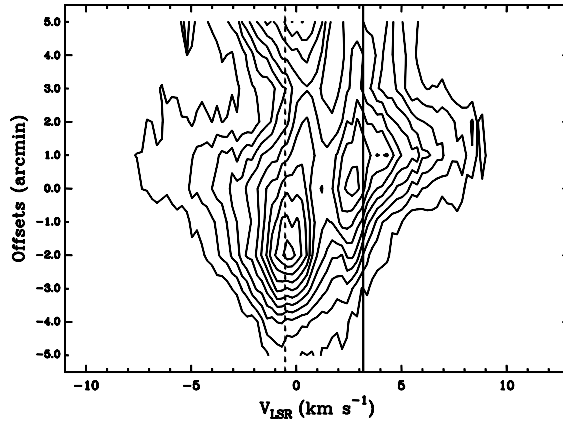
Fig. 2 Position-Velocity diagram constructed from the ^{12}CO J=2–1 transition. Contour levels are 1, 2, 3, 4.5, 6, 6.5, 7.5, 9, 10.5, 12, 14, ..., 25 K. The vertical dashed and solid lines indicate the beginning of the blueshifted and redshifted emission, respectively.

velocity components in Figure 2 further confirm a bipolar outflow in this region. Using the velocity ranges of the blueshifted and redshifted components, we made the integrated intensity map as shown in Figure 3.

In Figure 3, the blue and red contours represent the blueshifted and redshifted components of the outflow. The outflow clearly displays components in the north-southwest directions, which are associated with observations of HCO$^+$ J=2–1 and ^{13}CO J=1–0 emission lines (Little et al. 1988). The 1.4 GHz continuum emission is superimposed on the outflow, which may come from an HII region (Urquhart et al. 2009). Both the HII region and infrared source IRAS 20188+3928 are located in the beginning position of the outflow, but because of our low spatial resolution we cannot identify which object is the driving source of the outflow. An H$_2$O maser was detected in this region, which has the velocity of 1.1 km s^{-1} (Palla et al. 1991; Brand et al. 1994; Jenness et al. 1995). Comparing the components of the outflow, we find that the H$_2$O maser is not associated with the outflow, but with the core. If an accretion motion is further confirmed in this region, then the H$_2$O maser may come from the accretion disk of IRAS 20188+3928.

3.2.2 The outflow parameters

In this section, we use a large velocity gradient (LVG) radiative transfer model (Goldreich et al. 1974; Qin et al. 2008a) to determine the gas density (n(H$_2$)) and kinetic temperature (T_{kin}) of the outflow. The blueshifted and redshifted velocity intervals (Δv) are from -7.6 to -0.6 km s^{-1} and from 3.2 to 9.0 km s^{-1}, respectively. In this model, assuming a uniform density and using the above velocity intervals, n(H$_2$) and T_{kin} are obtained by fitting the line intensity of ^{12}CO J=2–1 and the line ratio of ^{12}CO J=3–2/^{12}CO J=2–1, which are varied over a reasonable range for this region.

Figure 4 shows the results of the LVG modeling. From Figure 4, various column densities are from 3.5×10^4 to 1.7×10^5 cm^{-3} with corresponding T_{kin} ranging from 22.9 to 30.9 K for the blueshifted lobe. The average values of possible n(H$_2$) and T_{kin} are 1.0×10^5 cm^{-3} and 26.9 K, respectively. For the redshifted lobe, n(H$_2$) ranges from 1.6×10^4 to 2.8×10^4 cm^{-3}, while T_{kin} is from 39.8 to 83.1 K. The averaged n(H$_2$) and T_{kin} are 2.0×10^4 cm^{-3} and 52.9 K, respectively.

Additionally, if both lobes are approximately spherical in shape, their mass is given by $M = n(\mathrm{H_2}) \frac{1}{6} \pi L^3 \mu_{\mathrm{g}} m(\mathrm{H_2})$ (Garden et al. 1991), where μ_{g}=1.36 is the mean atomic weight of the
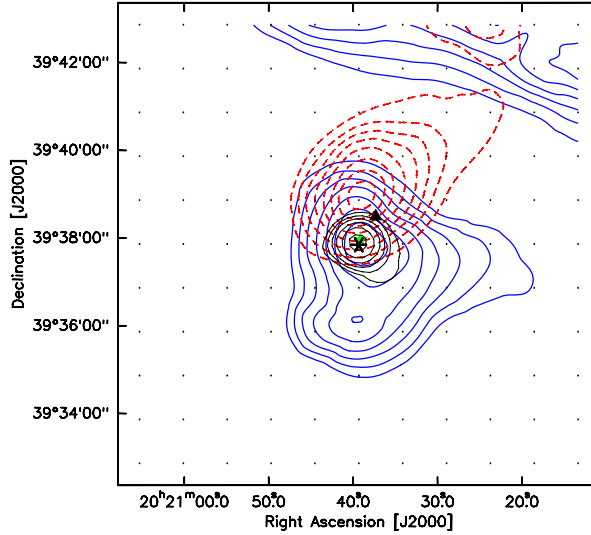
Fig. 3 The velocity-integrated intensity map of the ^{12}CO J=2–1 outflow (*red and blue contours*) overlaid with the 1.4 GHz emission (*black contours*). The black contour levels are at 3%, 6%, 9%, 12%, 15%, 18%, and 21 σ (1 σ is 0.002 Jy beam^{-1}). The red and blue contour levels are 35%, 50%, ..., 95% of the peak value. The H$_2$O maser is shown by a filled triangle. The "$*$" symbol indicates the position of IRAS 20188+3928 and the HII region. The green star shows the 2MASS source.

Table 1 Physical Parameters of the Outflow

Wing	T_{kin} (K)	$n(\mathrm{H_2})$ (10^5 cm^{-3})	M ($M_\odot$)	t_d (10^4 yr)	$\dot{M}$ (10^{-5} $M_\odot$ yr^{-1})	P ($M_\odot$ km s^{-1})	E (10^{44} erg)
Blue	26.9	1.0	3.3	5.6	5.9	11.6	4.0
Red	52.9	0.2	0.2	6.8	0.3	0.6	0.2

gas, L is the lobe diameter, and $m(\mathrm{H_2})$ is the mass of a hydrogen molecule. We calculate the dynamic timescales using $t_{\mathrm{d}} = r/v$, where v is the maximum flow velocity relative to the cloud's systemic velocity, and r is the length of the beginning-to-end flow extension for each lobe. The mass entrainment rate of the outflow is determined by $\dot{M} = M/(t_{\mathrm{d}})$. The momentum P and energy E are calculated by $P = MV$ and $E = MV^2$, where V is the mean velocity of the gas relative to the cloud's systemic velocity. The physical parameters and the calculated results of the outflow are listed in Table 1. A total mass and mass entrainment rate of the outflow are 3.5 $M_\odot$ and 6.2 $\times$ 10^{-5} $M_\odot$ yr^{-1}, respectively. The average dynamical timescale is about 6.2×10^4 yr.

3.2.3 *The integrated intensity ratio* ($I_{\mathrm{CO}\,J=3-2}/I_{\mathrm{CO}\,J=2-1}$)

The line intensity ratios based on the optically thick CO transitions can indicate the temperature varies at different positions (Qin et al. 2008b), and further trace shocks (Xu et al. 2011a,b; 2012). When the outflow comes into contact with the surrounding interstellar medium (ISM), this process can produce the shock. In order to obtain the integrated intensity ratio of ^{12}CO J=3–2 and J=2–1 ($I_{\mathrm{CO}\,J=3-2}/I_{\mathrm{CO}\,J=2-1}$), we convolved the 80$''$ of ^{12}CO J=3–2 data with an effective beam size of
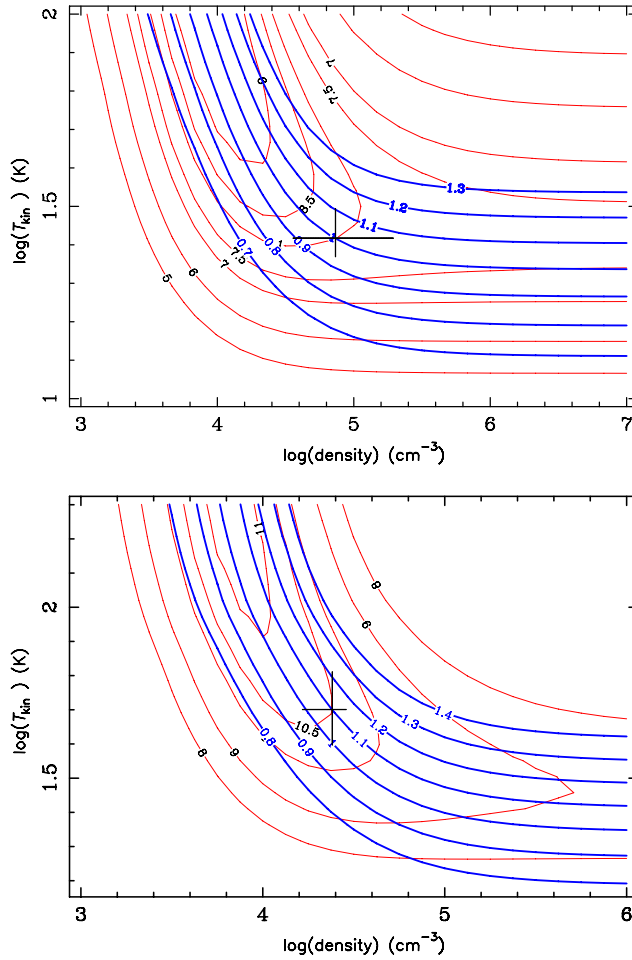
Fig. 4 LVG model analysis using the ^{12}CO J=2–1 and ^{12}CO J=3–2 lines. *Top*: The blueshifted components of the outflow. *Bottom*: The redshifted components of the outflow. The horizontal and vertical axes are the volume density n_{H_2} and kinetic temperature T_{kin} in log scale, respectively. Blue thick curves represent line intensity of ^{12}CO J=2–1, while red thin curves represent the line ratios of CO(J=3–2)/CO(J=2–1). The results of T_{kin} and n_{H_2} are taken from the crossing points of the red and blue curves. The error bars indicate the range of possible solutions.

$\sqrt{130^2 - 80^2} = 102''$. The integrated intensities were calculated for the ^{12}CO J=2–1 line in the same velocity range as for ^{12}CO J=3-2.

Figure 5 shows the distribution of the ratio (color scale) overlaid with the distribution of the ^{12}CO J=2–1 line integrated intensity of the outflow (black solid and dashed contours). From Figure 5, we can see that the distribution of both ratios presents shell-like morphology. The maximum ratio value is 1.2 in the blueshifted lobe, while the redshifted lobe has the maximum ratio value of 1.7. The rms level is 0.10 (1σ). The molecular clouds associated with HII regions have a higher ratio and a higher gas temperature than those sources without HII regions, indicating that the high line ratio may be due to heating of the gas by massive stars (Wilson et al. 1997). The high ratio values
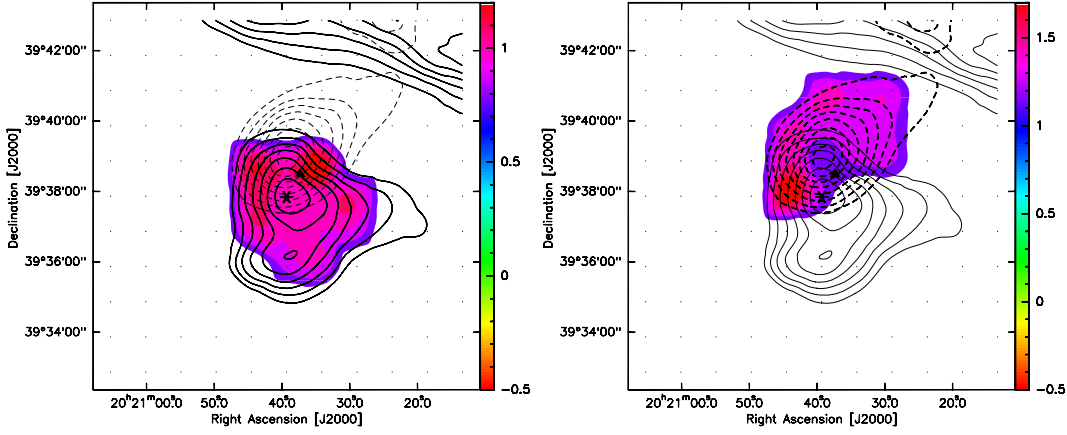
Fig. 5 ^{12}CO J=2–1 intensity maps of the outflow are superimposed on the line intensity ratio maps (color scale). The filled triangle indicates the line-intensity ratio scale. The "∗" symbol indicates the position of IRAS 20188+3928 and the HII region. *Left panel*: the blueshifted lobe; *Right panel*: the redshifted lobe.

in molecular clouds interacting with a supernova remnant (SNR) (Xu et al. 2011a,b; 2012) exceed previous measurements of individual Galactic molecular clouds, implying that the SNR shock has driven into the molecular clouds. Here, the high ratio values detected in the region of the outflow may be caused by the outflow interacting with the surrounding ISM. In addition, because the maximum value of the ratio of the redshifted lobe is greater than that of the blueshifted lobe, we suggest that the redshifted lobe has a higher temperature, which is related to the results derived from the LVG model. In Section 3.2.2, we find that the redshifted lobe has a kinetic temperature of 52.9 K, which is larger than that (26.9 K) of the blueshifted lobe.

4 CONCLUSIONS

We present submillimeter/millimeter observations of the high-mass protostellar candidate IRAS 20188+3928 in the ^{12}CO J=2–1 and ^{12}CO J=3–2 lines. The spectral profiles of ^{12}CO J=2–1 and ^{12}CO J=3–2, with both showing an absorption dip, together with the ^{13}CO J=1–0 line featuring a single peak profile, indicate that possible rotation may be associated with IRAS 20188+3928. The ^{12}CO J=2–1 velocity-integrated intensity map, position-velocity diagram, and the broad wing (FW = 20 km s^{-1}) of the ^{12}CO J=2–1 line further verify that there is an outflow motion. The outflow emission is elongated along the north-southwest direction. This region is also associated with an HII region and an IRAS source, but we cannot identify which object is the driving source of the outflow due to our lower spatial resolution. An H$_2$O maser is also associated with this region. Compared with the components of the outflow, we find that the H$_2$O maser is not associated with the outflow, but may be associated with the core of IRAS 20188+3928. Using the LVG model, the possible kinetic temperatures of the blueshifted lobe and redshifted lobe are 26.9 K and 52.9 K, respectively. The total gas mass, average dynamical timescale, and mass entrainment rate of the outflow are 3.5 $M_{\odot}$, 6.2 × 10^4 yr and 6.2 × 10^{-5} $M_{\odot}$ yr^{-1}, respectively. The outflow has a higher integrated intensity ratio ($I_{\rm CO\,J=3-2}/I_{\rm CO\,J=2-1}$), which may be caused by the outflow interacting with the surrounding ISM. Because the maximum value of the ratio of the redshifted lobe is greater than that of the blueshifted lobe, we suggest that the redshifted lobe has the higher temperature.

References

Anglada, G., Sepulveda, I., & Gomez, J. F. 1997, A&AS, 121, 255

Brand, J., Cesaroni, R., Caselli, P., et al. 1994, A&AS, 103, 541

Condon, J, J., Cotton, W. D., Greisen, E. W., et al. 1998, AJ, 115, 1693

Fich, M., Blitz, L., & Stark, A. A. 1989, ApJ, 342, 272

Garden, R. P., Hayashi, M., Hasegawa, T., Gatley, I., & Kaifu, N. 1991, ApJ, 374, 540

Goldreich, P., & Kwan, J. 1974, ApJ, 189, 441

Jenness, T., Scott, P. F., & Padman, R. 1995, MNRAS, 276, 1024

Jijina, J., Myers, P. C., & Adams, F. C. 1999, ApJS, 125, 161

Little, L. T., Bergman, P., Cunningham, C. T., et al. 1988, A&A, 205, 129

Molinari, S., Brand, J., Cesaroni, R., & Palla, F. 1996, A&A, 308, 573

Molinari, S., Brand, J., Cesaroni, R., Palla, F., & Palumbo, G. G. C. 1998, A&A, 336, 339

Palla, F., Brand, J., Comoretto, G., Felli, M., & Cesaroni, R. 1991, A&A, 246, 249

Qin, S.-L., Zhao, J.-H., Moran, J. M., et al. 2008a, ApJ, 677, 353

Qin, S.-L., Wang, J.-J., Zhao, G., Miller, M., & Zhao, J.-H. 2008b, A&A, 484, 361

Urquhart, J. S., Hoare, M. G., Purcell, C. R., et al. 2009, A&A, 501, 539

Varricatt, W. P., Davis, C. J., Ramsay, S., & Todd, S. P. 2010, MNRAS, 404, 661

Wilson, C. D., Walker, C. E., & Thornley, M. D. 1997, ApJ, 483, 210

Wu, J., Evans, N. J., II, Shirley, Y. L., & Knez, C. 2010, ApJS, 188, 313

Wu, Y., Zhu, M., Wei, Y., et al. 2005, ApJ, 628, L57

Xu, J.-L., & Wang, J.-J. 2012, A&A, 543, A24

Xu, J.-L., Wang, J.-J., & Miller, M. 2011a, ApJ, 727, 81

Xu, J.-L., Wang, J.-J., & Miller, M. 2011b, RAA (Research in Astronomy and Astrophysics), 11, 537

Yao, Y., Ishii, M., Nagata, T., Nakaya, H., & Sato, S. 2000, ApJ, 542, 392

Zhang, Q., Hunter, T. R., Brand, J., et al. 2005, ApJ, 625, 864